

# Regulating electronic properties of BiOBr to enhance visible light response via 3d transition metals doping: DFT+U calculations

Meihua Guan<sup>1</sup>, Guangmin Ren<sup>1</sup>, Xiaochao Zhang<sup>1</sup>, Qirui Zhang<sup>1</sup>, Changming Zhang<sup>1</sup>, Rui Li<sup>1</sup>, and Caimei Fan<sup>1</sup>

<sup>1</sup>Taiyuan University of Technology

August 11, 2020

## Abstract

In our work, the formation energies, band structures, densities of states, effective masses and optical absorption properties of pure BiOBr and 3d transition metals-doped BiOBr have been calculated using DFT+U method. Ti, V, Fe, Cr, Co, Ni and Cu doping can induce impurity energy levels, originating from spin-up or -down orbits of 3d TMs, within the forbidden band of BiOBr, but Sc, Mn and Zn atoms only change the electronic delocalization in the valence band or conduction band region of BiOBr. Furthermore, with introduction of 3d TMs atoms, there exist the redshift phenomena for optical absorption band edge of BiOBr to different extents. The photo response priority order, structural stability and recombination probability of photoinduced carriers for 3d TMs-doped BiOBr are summarized. Our theoretical findings should well explain the experimental observations in the previous literatures, and provide promising prediction and significant guidance for the well-construction of BiOBr-based photocatalyst systems.

## Regulating electronic properties of BiOBr to enhance visible light response via 3d transition metals doping: DFT+U calculations

Meihua Guan<sup>1</sup>, Guangmin Ren<sup>1</sup>, Xiaochao Zhang<sup>1,\*</sup>, Qirui Zhang<sup>1</sup>, Changming Zhang<sup>2</sup>, Rui Li<sup>1</sup>, Caimei Fan<sup>1,\*</sup>

<sup>1</sup>College of Chemistry and Chemical Engineering, Taiyuan University of Technology, Taiyuan 030024, PR China

<sup>2</sup>College of Mining Engineering, Taiyuan University of Technology, Taiyuan 030024, PR China

## CORRESPONDING AUTHOR :

**Xiaochao Zhang** , College of Chemistry and Chemical Engineering, Taiyuan University of Technology, Taiyuan 030024, PR China. **Tel.** : +86-15503477962; **Fax** : +86-351-6018554. **E-mail** : zhangxiaochao@tyut.edu.cn, fancm@163.com.

**ACKNOWLEDGMENTS** This work is supported by the National Natural Science Foundation of China (No. 21978196, 21676178, 21706179) and Shanxi Province Science Foundation for Excellent Youths (201801D211008), Scientific and Technological Innovation Project of Higher Education Institutions in Shanxi (201802051).

## AUTHOR CONTRIBUTIONS

**Meihua Guan** : Data curation; formal analysis; investigation and writing-original draft. **Guangmin Ren** : Methodology. **Xiaochao Zhang** : Conceptualization; writing-review; editing and resources. **Qirui Zhang** : Investigation. **Changming Zhang** : Investigation; supervision. **Rui Li** : Investigation; supervision. **Caimei Fan** : Methodology; resources.

**Abstract:**In our work, the formation energies, band structures, densities of states, effective masses and optical absorption properties of pure BiOBr and 3d transition metals-doped BiOBr have been calculated using DFT+U method. Ti, V, Fe, Cr, Co, Ni and Cu doping can induce impurity energy levels, originating from spin-up or -down orbits of 3d TMs, within the forbidden band of BiOBr, but Sc, Mn and Zn atoms only change the electronic delocalization in the valence band or conduction band region of BiOBr. Furthermore, with introduction of 3d TMs atoms, there exist the redshift phenomena for optical absorption band edge of BiOBr to different extents. The photo response priority order, structural stability and recombination probability of photoinduced carriers for 3d TMs-doped BiOBr are summarized. Our theoretical findings should well explain the experimental observations in the previous literatures, and provide promising prediction and significant guidance for the well-construction of BiOBr-based photocatalyst systems.

**KEYWORDS :** Density Functional Theory; BiOBr; 3d transition metals; electronic structure; optical property

## 1. INTRODUCTION

In the past few decades, increasing concerns had been paid for energy crisis and environmental pollution issues, and photocatalysis technology, as a promising route for renewable energy development and environmental governance, has drawn more and more attentions<sup>[1]</sup>. BiOBr, was deemed as the most promising photocatalyst due to the special structure-dependent photocatalytic performance, excellent chemical stability and environmental-friendly quality<sup>[2]</sup>, it possessed a lamellar structure, which can offer enough space for polarizing the corresponding atoms and orbitals and provide self-built internal electric field (IEF), and consequently, obtaining that the induced dipole could accelerate efficiently the separation and migration of photoinduced electron-hole ( $e^- - h^+$ ) pairs, improving the photocatalytic performance<sup>[3-5]</sup>. More importantly, BiOBr shows an appropriate indirect band gap, implies that photogenerated  $e^-$  must cross a certain  $k$ - space to be emitted to CB, further to prevent the recombination rates of photoexcited  $e^- - h^+$  pairs<sup>[5, 6]</sup>. Nevertheless, there exist low quantum efficiency and fast photoexcited  $e^- - h^+$  pairs recombination rates as the “bottleneck” for satisfying with the requirement of practical applications<sup>[7, 8]</sup>. Therefore, it is rather critical to explore novel strategies to improve the photocatalytic performance of BiOBr.

In recent years, domestic and foreign scientists based on the basic principles of semiconductor photocatalysis, from three aspects of expanding light absorption, improving carrier separation efficiency and enhancing surface interaction to strengthen the photocatalytic reaction<sup>[9]</sup>, and among the normal modification strategies, the construction of doping systems<sup>[10-15]</sup> is one of the most representative ways to enhance visible-light response and improve photocatalytic activity of BiOBr. TMs doping may induce potential electron traps to prolong the lifetime of photoexcited carriers and introduce magnetic feature, as well as change energy band structure to increase light absorption ability and adjust the redox potentials, thus TMs-doped BiOBr used to obtain high photocatalytic activity<sup>[16]</sup>. For instances, Wang et al. adopted double self-assembly method to successfully synthesize Ti-doped BiOBr photocatalyst with more superior photocatalytic activity than undoped BiOBr in terms of degrading RhB, attributing to the synergetic effect of larger specific surface area, unique microspheres structure and Ti doping<sup>[10]</sup>. Jiang et al. reported a Ti doping and Ag decorating BiOBr microsphere with excellent photocatalytic activity and durability<sup>[11]</sup>. For Fe-doped BiOBr photocatalysts, Fe ions played key role for doping effect in the self-assembly process of hollow microspheres, revealing high photocatalytic and electrochemical performance<sup>[13]</sup>. Recently, Guo et al. utilized experimental and DFT methods to investigate Zn-doped BiOBr system, and theoretical calculations reveal that there still maintain the advantages of indirect band gap after the introduction of Zn, and Zn 3d states with deeper energy levels could induce negligible effect on VB and CB of Zn-doped BiOBr system<sup>[15]</sup>. Furthermore, DFT calculations were adopted to evaluate the influence of Co doping on the electronic structure of BiOBr by Xia et al., revealing that there is an additional energy level introduced into the forbidden band of Co-doped BiOBr system<sup>[17]</sup>. Based on above-mentioned results, it could be inferred that the doping of 3d TMs should affect the electronic and optical properties as well as macro-performances of BiOBr to a certain extent.

However, there are few reports about exploring a series of 3d TMs doped modulation electronic structures to influence the micro- and macro- properties as well as both correlations and redox potentials of BiOBr.

Motivated by the previous experimental and theoretical achievements<sup>[15-18]</sup>, we investigate carefully and systematically the electronic structure of 3d TMs-doped BiOBr using DFT+U calculations. Given our theoretical findings, it is to clarify that how the electronic structure influence visible light absorption and provide possible explanations for previous experimental observations, more importantly, also could provide significative guidance to synthesize BiOBr-based materials with highly photocatalytic activity.

## 2. COMPUTATIONAL MODELS AND DETAILS

### 2.1. Computational models

BiOBr belongs to tetragonal crystal, and its space group is P4/nmm (NO.129)<sup>[19]</sup>. The atoms of primitive cell occupy the following special positions: O in 2a (0, 0, 0), Br in 2c with a fractional parameter  $u_{\text{Br}}$ (0, 0.5, 0.653) and Bi also in 2c but with a different parameter  $u_{\text{Bi}}$ (0, 0.5, 0.154). BiOBr crystal is composed by alternative stacks of double Br slabs and  $[\text{Bi}_2\text{O}_2]^{2+}$  slabs along [001] direction into a tetragonal matlockite (PbFCl) structure<sup>[20]</sup>. In order to study the influence of electronic structure regulation visible-light response via 3d TMs doping BiOBr, we adopted  $3 \times 2 \times 2$  supercell with 72 atoms, because excessive metal doping may induce the appearance of new recombination traps of photogenerated  $e^- - h^+$  pairs<sup>[18]</sup>. Here, 3d TMs-doped BiOBr systems are built up through replacing one Bi atom located at the host of BiOBr crystal lattice with 3d TM atom, corresponding to 4.167% atomic doping content, as illustrated in Figure 1. The introduced TMs atoms are more biased towards the O atom layer, which may be attributed to the substitution of smaller radius for 3d TMs than Bi atom  $r_{\text{Bi}}=1.17 \text{ \AA}$ <sup>[12]</sup>.

### 2.2. Calculational details

All of the calculations are carried out using plane-wave pseudopotential DFT+U method in “CASTEP” module, which is developed by Accelrys Company<sup>[21]</sup>, the exchange correlation energy were treated based on the GGA with PBE functional<sup>[22]</sup>, with the considerations of spin-orbit polarization. In the simulation, the core electrons were treated with the ultrasoft pseudopotential, and the configurations of valence electrons were selected as Bi  $6s^2 6p^3$ , O  $2s^2 2p^4$ , Br  $4s^2 4p^5$ , Sc  $3d^1 4s^2$ , Ti  $3d^2 4s^2$ , V  $3d^3 4s^2$ , Cr  $3d^5 4s^1$ , Mn  $3d^5 4s^2$ , Fe  $3d^6 4s^2$ , Co  $3d^7 4s^2$ , Ni  $3d^8 4s^2$ , Cu  $3d^{10} 4s^1$ , Zn  $3d^{10} 4s^2$ . The plane-wave cut-off energy of 500 eV and a Monkhorst-Pack  $3 \times 3 \times 3$   $k$ -point grid were used. In addition, the convergence standards were set as the follows: the force and stress were less than 0.5 eV/Å and 0.1 Gpa, respectively as well as the energy change was less than  $2 \times 10^{-5}$  eV/atom<sup>[18]</sup>. More importantly, we adopted DFT+U approach to overcome the disadvantage of GGA-PBE due to the nonnegligible d-d transition of transition metal<sup>[23, 24]</sup>. As we all know, a finite onsite Coulomb interaction is essential for accurately describing atoms containing d electrons<sup>[25]</sup>, so the on-site Coulomb interaction with  $U=4.0$  eV is used in the calculations<sup>[26]</sup>. In order to make the calculated optical properties results consistent with the actual situation, “scissors operators” technology<sup>[27]</sup> was adopted, and the correction factor was set as 0.8 eV in our work, which is based on the deviation of the calculated values and the experimental data of average band gap.

## 3. RESULTS AND DISCUSSION

### 3.1. Electronic properties of pure BiOBr

In order to confirm the influence of electronic structure on visible-light response of BiOBr within and without the doping of 3d TMs (TMs=Sc, Ti, V, Cr, Mn, Fe, Co, Ni, Cu, Zn), the relaxed atomic structure with  $3 \times 2 \times 2$  BiOBr supercell is deemed as the basic research subject. The obtained lattice constants after geometry optimization are  $a = b = 3.909 \text{ \AA}$ ,  $c = 8.678 \text{ \AA}$ , in accordance with the previously reported literatures<sup>[24, 28]</sup>. The electronic band structure of BiOBr supercell is projected in the Brillion zone, as shown in Figure 2(a). Generally, the zero of energy axis is set as Fermi level ( $E_f$ ).

The calculated band gap ( $E_g$ ), the distance between valence-band maximum (VBM) and conduction-band minimum (CBM), of  $3 \times 2 \times 2$  BiOBr supercell is 2.173 eV using DFT+U method, smaller than the experimental value 2.6~2.9 eV<sup>[29, 30]</sup>, which is caused by the well-known inherent shortcomings of GGA-PBE functional<sup>[31]</sup>. Since the carrier effective mass and mobility are directly related to the band wave curvature, it can be seen that the electronic energy levels at CBM of BiOBr are high dispersive, revealing that the

smaller effective mass and higher mobility of photoinduced  $e^-$  in CBM. Besides, VBM is the between  $G$  and  $F$  point, yet CBM is located at  $G$  point, which belong to the various locations in the Brillouin zone and exhibit the indirect bandgap characteristic of BiOBr with special bandgap transition pathway that photo-generated  $e^-$  will be transited from VB to CB through a certain  $k$ -space and leave  $h^+$  on VB, which should inhabit the recombination rates of photogenerated  $e^-h^+$  pairs and improve the photocatalytic performance effectively<sup>[5, 6]</sup>.

Figure 2(b) illustrates the calculated total density of states (TDOS) and projected densities of states (PDOSs) of BiOBr. Calculations indicate that the VBM of BiOBr is mainly determined by Br 4p and O 2p states, whereas CBM is mainly determined by Bi 6p states and a small contribution of Bi 6s electron states, therefore, pure BiOBr might belong to the p-to-p (O 2p and Br 4p to Bi 6p) charge-transfer type. Our analysis results of electronic structure are in good agreement with the previous published results using DFT approach, revealing that the adopted calculation method and obtained results should be reasonable and credible<sup>[28, 32]</sup>.

### 3.2. No impurity levels of 3d transition metals in BiOBr forbidden band

As shown in Figure 3(a), compared with TDOS spectra of Sc, Mn, Zn-doped BiOBr and pure BiOBr, the calculated forbidden band widths of Sc-, Mn- and Zn-doped BiOBr are 2.200 eV, 2.105 eV, 2.112 eV, respectively, very closer to the bandgap (2.173 eV) of BiOBr, and the introduction of Sc, Mn or Zn atom has no effect on indirect-band-gap characteristic of BiOBr. Additionally, there is no IELs appearing in the forbidden band of Sc-, Mn-, Zn-doped BiOBr. Meanwhile, the PDOSs of Sc-, Mn- and Zn-doped BiOBr are shown in Figure 3 (b-d). It is found that Mn 3d up-spin states mainly contribute to VBM and occupy VB with a bandwidth of 5.54 eV, which will trap photoexcited  $h^+$ , enhancing the separation efficiency of photogenerated carriers in the Mn-doped BiOBr system to a certain extent<sup>[16]</sup>. Meanwhile, the previous experimental work indicated that the introduction of Mn could bring about oxygen vacancies to obtain more active sites on the BiOBr surface<sup>[33]</sup>, the reasons why is that both of Mn-doped BiOBr<sup>[12]</sup> and BiOBr-Mn<sub>3</sub>O<sub>4</sub> nanoheterojunction photocatalysts<sup>[34]</sup> exhibited the higher photocatalytic performance than pure BiOBr.

For Sc-, Zn-doped BiOBr, 3d up and down spin states of Sc and Zn atoms in the energy band are symmetric, indicating that the total magnetic moment of BiOBr system is still zero after the introduction of Sc or Zn atom, associated with their relatively stable outermost electron configurations of Sc 3d<sup>1</sup>4s<sup>2</sup> and Zn 3d<sup>10</sup>4s<sup>2</sup>. Furthermore, the introduction of Sc results in the bandgap increase from 2.173 to 2.200 eV, indicating that required photon energy to excite  $e^-$  transition of Sc-doped BiOBr system, higher than BiOBr. Similarly, for Zn-doped BiOBr system, there is no IELs observed within the forbidden band, because  $e^-$  on closed 3d orbitals of Zn atom is not interactive to offer electronic states to band gap<sup>[15]</sup>. Obviously, there is a significant variability in the electron contribution of Zn 3d states compared with Sc and Mn 3d states. Zn 3d up- and down-spin states contribute to deeper energy levels in VB, lower than VBM, locating at the range of -3~-6 eV with much better oxidizability, consistent with reported experimental findings of Zn-doped BiOBr system by Guo et al.<sup>[15]</sup>.

To further comprehend the doping effects of 3d TMs on the optical properties of BiOBr, the optical absorption spectrums for BiOBr and Sc, Mn, Zn-doped BiOBr are shown in Figure 4. Pure BiOBr shows a wide light response range with an absorption edge at 448 nm, corresponding to a band gap value of 2.9 eV, whereas there is no obvious effects in case of Sc- or Zn-doped BiOBr. Therefore, we believe that Sc or Zn doping only affect the electronic localization in the region of VB or CB, has negligible influence on the optical properties of BiOBr. However, for Mn-doped BiOBr system, the absorption intensity between 450 and 800 nm has an obvious enhancement compared with pure BiOBr, and the visible-light response is enhanced, which may be attributed to the contribution of Mn 3d states to VB. The above calculation results are in good accordance with the pervious published references<sup>[12, 15, 35]</sup>.

### 3.3. Impurity levels of 3d transition metals in BiOBr forbidden band

The TDOSs of BiOBr and Ti-, V-, Fe-, Cr-, Co-, Ni-, Cu-doped BiOBr were plotted in Figure 5 within the range of -6 to 5 eV. It is found that the electronic structural features of pure BiOBr remain intact

except for the appearance of IELs, which mainly originate from TMs 3d electron states, within the BiOBr forbidden band. In general, the present of IELs could provide more photoexcited charge carriers under the condition of less absorption energy than pure BiOBr<sup>[36]</sup>, leading to a repression in the recombination rates of photogenerated  $e^-h^+$  pairs and an improvement in the optical absorption ability. Besides, except for Ni-doped BiOBr system, the band gaps of other TMs doped BiOBr increase to the different extents, and the shift of relative positions for VBM and CBM occurs, leading insuperably to the change of redox potentials of BiOBr. Surprisingly, all the doping systems still retain an indirect-band-gap advantage of BiOBr, suppressing the recombination probability of photoinduced  $e^-h^+$  pairs.

The calculated band gaps of Ti-, V-, Fe-, Cr-, Co-, Ni-, Cu-doped BiOBr are 2.206, 2.203, 2.197, 2.193, 2.195, 2.171, 2.189 eV, respectively. The increased band gaps contribute to the improvement of redox capability and the enhancement of separation efficiency for photogenerated  $e^-h^+$  pairs, however, the band gap of Ni-BiOBr system is only narrowed slightly. In addition, the VBMs of V-, Fe-, Co-, Ni-, Cu-doped BiOBr shift to the more negative direction, locating at -0.406, -0.448, -0.351, -0.176, -0.270 eV, respectively, revealing that the oxidation abilities of these doped-BiOBr systems exhibited a significant enhancement after the introduction of V, Fe, Co, Ni, Cu atoms, the reasons are why that such reported as-prepared photocatalysts demonstrate excellent photocatalytic activity in terms of degrading organic pollutants<sup>[13, 14, 37, 38]</sup>.

The PDOSs of Ti-, V-, Cr-, Fe-, Co-, Ni-, Cu atoms in such doping BiOBr are calculated and shown in Figure 6 (a-g). For Ti-, V-, Fe-doped BiOBr, the PDOSs of Ti, V, Fe atoms show the similar 3d electron states distribution. Ti 3d states mainly contribute to CBM and CB with bandwidth of 1.37 4.05 eV, as well as a small contribution for VB, nevertheless, there is an IEL (at 1.641 eV within the forbidden band), which originating from Ti 3d down-spin state forms, exhibiting an  $n$ -type semiconductor property, which should help photoexcited  $e^-$  transfer to more reactive sites of catalyst under light irradiation. Doping V into BiOBr crystal will induce two IELs located at -0.116 and 1.797 eV, originating from V 3d down-spin states. For Fe-doped BiOBr system, two obvious IELs located at 0.966 and 1.468 eV are from the contribution of Fe 3d down-spin states. Meanwhile, Fe 3d down-spin states have higher density and localized distribution than Ti and V. As everyone knows, appropriate depth of IELs will play an important role in the transition process of proton, so the IELs in the Fe-doped BiOBr system should act as a springboard for electron transitions from the VB to CB, and then provide more photoexcited  $e^-$  to CBM and more  $h^+$  to VBM, improving the separation of photoexcited charge carriers effectively. Experimentally, a novel Fe<sup>3+</sup>-doped BiOBr magnetic Janus micromotors, which has excellent solar Fenton catalytic activity, was reported by Liu and co-workers<sup>[39]</sup>. More worthy of reference for the theoretical explains of such previous experiments, novel super paramagnetic BiOBr/Fe<sub>3</sub>O<sub>4</sub> was fabricated via an in-situ growth method that can easily achieve the norfloxacin (NOR) recovery from solution<sup>[40]</sup>.

As displayed in Figure 6(d-f), the PDOSs of Cr, Co, Ni atoms exhibit the similar distribution characteristics of electronic states. Their 3d up- and down-spin electronic states mainly contribute to VB and IELs, and surprisingly, with their outermost electron configurations gradual increase, the distances between the IELs (3d down-spin states) and VBM are reduced from 2.193 to 0.397 eV, and the localization of 3d down-spin states gradually weakens, it should be because of the high occupancy of d-orbitals can lower the energy of d electron states, thus moving the IELs away from CB and contributing to the VBM, which maybe lead to a redshift of optical absorption edge.

For the PDOSs of Cu atoms plotted in Figure 6(g), Due to the stable outermost electron configuration, Cu 3d states show the symmetric up- and down-spin. There exists an IEL located at 0.308 eV, dominating by Cu 3d electron states. The emergence of new IEL with the stronger density slightly above VBM can make the electronic transition from the original one-step excitation to two-step process, consequently, reducing photocatalytic threshold and extending the light absorption range.

We adopted electric dipole approximation to calculate optical properties. The probability of a linear transition between occupied and unoccupied states excited by photons is determined by the electronic structure<sup>[42]</sup>. Figure 7 shows the calculated absorption spectrum of BiOBr and Ti-, V-, Fe-, Cr-, Co-, Ni-, Cu-doped BiOBr. Due to inter-band absorbance, pure BiOBr has an absorption band edge at 448 nm and a wide optical re-

sponse range. After the TMs atom incorporated into BiOBr, the optical absorption band edges exhibit the redshift to different extents, in particular, Fe-, Co-, Ni-, Cu-doped BiOBr have obvious tail that can expand absorption in the visible-light region of 400-800 nm<sup>[43]</sup>, surprisingly, Liu reported that Fe<sup>3+</sup>-doped BiOBr exhibited an obvious shift toward long wavelength region compared to pure BiOBr experimentally, in agree with our theoretical results<sup>[39]</sup>. Firstly, the narrower band gap facilitates electronic transitions by absorbing low-energy photons, enhancing light harvesting capacity, such as Ni-doped BiOBr catalysts. IELs, which appear in the bandgap, then could act as footstep in the electronic transition, causing the electronic transition from original one-step excitation to two-step process, or even multi-step excitation, resulting in a lower threshold for photoexcitation between the VBM and CBM, owing to higher oxidation states of the 3d TMs ions required for charge compensation<sup>[44]</sup>. In addition, Cu with localized surface plasmon resonance (LSPR) could effectively improve the collection and conversion of light energy. These are the three main reasons why those optical properties are improved after the incorporation of 3d TMs into BiOBr crystal. Therefore, it can be speculated that if V-, Cr-, Ni-, Cu-doped BiOBr photocatalyst are prepared experimentally, it will be obtained such similar enhanced visible light response and performances.

When additional atoms are introduced into crystal lattice, the association between outer-shell orbitals of these atoms and energy band electronic states induces IELs, and regulate the electronic structures. In order to clearly illustrate the effect of modulation of the electronic structure on the light response and redox potential after the introduction of the 3d TMs, Figure 8 shows the electronic energy level distribution position and light absorption condition of 3d TMs-doped and pure BiOBr. On the one hand, the VBM shifts to more negative direction than pure BiOBr when V, Fe, Co, Ni, Cu atoms are inserted into BiOBr crystal lattice, and consequently, obtaining more excellent oxidation ability, the analysis results of the Fe- and Co-doped BiOBr catalysts are good consistent with previous reports in the literature<sup>[7, 16]</sup>. On the other hand, due to the change in the electronic structure via 3d TMs doping, the Mn-, Fe-, Co-, Ni-, Cu-doped BiOBr obtain strong visible-light absorption, and the absorption band edge of Ti-, V-, Cr-doped BiOBr exhibit a redshift.

### 3.4. Charge carriers separation efficiency and structural stability of 3d TMs-dopedBiOBr

To further investigate charge separation efficiency, the effective masses of photogenerated charge carriers of 3d TMs-doped BiOBr were calculated based on our obtained results of electronic structure. All the calculations about the effective mass of  $e^-$  and  $h^+$  according to the following equation:

$$m^* = \pm \frac{\hbar}{d^2 E / dk^2} \quad (1)$$

where  $m^*$  is the effective mass of photoexcited charge carriers,  $\hbar = h/2\pi$ ,  $h$  is the planck constant and  $d^2 E / dk^2$  is the coefficient of quadratic term in quadratic fit of  $E(k)$  curves for band edge<sup>[45]</sup>. Meanwhile, the relative ratio ( $D$ ) of effective masses can be evaluated via an equation:  $D = \frac{m_h^*}{m_e^*}$ , where  $m_h^*$  and  $m_e^*$  represent the effective mass of  $h^+$  and  $e^-$ , respectively<sup>[42]</sup>. In general, the higher values of  $D$  imply a lower recombination probability of photogenerated  $e^-h^+$  pairs, and the smaller effective masses of photoinduced  $h^+$  or  $e^-$  suggest that carriers have the higher delocalization and mobility. The calculated effective mass of  $h^+$  and  $e^-$  as well as  $D$  of 3d TMs-doped BiOBr are illustrated in Table 1. It is easy to find that the  $D$  value of Mn-, Ni-, Zn-doped BiOBr is higher than other systems, confirming that the recombination rates of photogenerated  $e^-h^+$  pairs decrease after the introduction of Mn, Ni, Zn atoms, consistent with the analysis results from the PDOS of Mn-doped BiOBr system. Surprisingly, for Fe-doped BiOBr system, the effective mass of charge carriers diminishes slightly, indicating the greater mobility of photogenerated  $e^-$  and  $h^+$  than pure BiOBr, then the carriers will reach to surface reaction sites within the lifetime easily, which is why that Fe-doped BiOBr samples had superior highly-efficient photocatalytic performance<sup>[19]</sup>.

It is well known that the structure stability is a significant parameter for evaluating the performance of photocatalytic material. Formation energies are calculated to judge thermodynamic stability of doping systems and ensure the most suitable doping site, importantly, theoretical calculated results can guide the preparation of structurally stable photocatalysts in the experiment<sup>[46]</sup>. That being the case, we calculated  $E_{\text{form}}$  of 3d TMs-doped BiOBr by the following equation:

$$E_{\text{form}} = E_{\text{TM-BiOBr}} - (E_{\text{BiOBr}} + E_{\text{TM}} - E_{\text{Bi}}) \quad (2)$$

where  $E_{\text{BiOBr}}$ ,  $E_{\text{TM-BiOBr}}$ ,  $E_{\text{TM}}$  and  $E_{\text{Bi}}$  represent the total energy of BiOBr, 3d TMs-doped BiOBr, an isolated 3d TMs and Bi atom, respectively<sup>[17]</sup>. The  $E_g$  and  $E_{\text{form}}$  of 3d TMs-doped BiOBr were tabulated in Table 2.

The formation energies of Ni-, Cu-, Zn- doped BiOBr are 0.781, 3.174 and 4.199 eV, respectively, indicating that it is an endothermic reaction when Ni, Cu, Zn atoms replace Bi atom into BiOBr lattice. In contrast, the formation energies of Sc-, Ti-, V-, Cr-, Mn-, Fe-, Co-doped BiOBr are -4.721, -4.187, -3.707, -3.794, -3.182, -1.993, -0.013 eV, respectively, implying the structure stability of Sc, Ti, V, Cr, Mn, Fe, Co-doped BiOBr catalysts, some systems have been reported by the research group<sup>[10, 12-14]</sup>. According to calculated results of such formation energies, we can also intuitively understand the priority order of 3d TM atoms substituting Bi atom into BiOBr crystal lattice: Sc>Ti>Cr>V>Mn>Fe>Co>Ni>Cu>Zn, associated with their atomic radius. Finally, in order to clarify the relationship between the forbidden band width and structure stability of 3d TMs-doped BiOBr, we plotted their relevance diagram in Figure 9.

In order to intuitively reveal the doping effect of 3d TMs on photo response, structural stability and recombination probability of photoinduced carriers of BiOBr, based on the calculation results, a 3D scatter plot has been drawn in Figure 10. The three coordinates after the 3d TMs represent their priority order in inhibit charge carrier recombination, structural stability and light response, respectively. For example, the coordinates of the Mn-doped system are (2, 5, 2), indicating that the introduction of Mn atom could inhibit the recombination of photogenerated  $e^- - h^+$  pairs effectively and enhance visible light absorption significantly, while the thermodynamic stability of such system is not outstanding. Our findings should provide theoretical guide for experimenters to design novel photocatalytic material with extensive application prospects.

#### 4. CONCLUSION

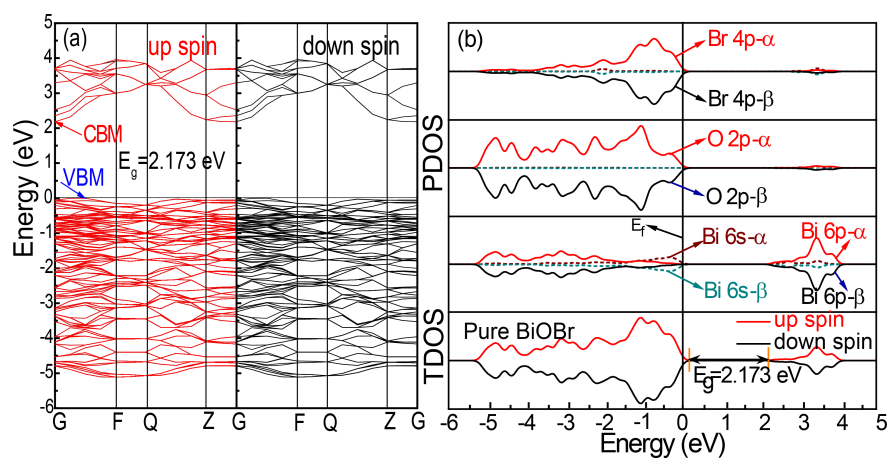
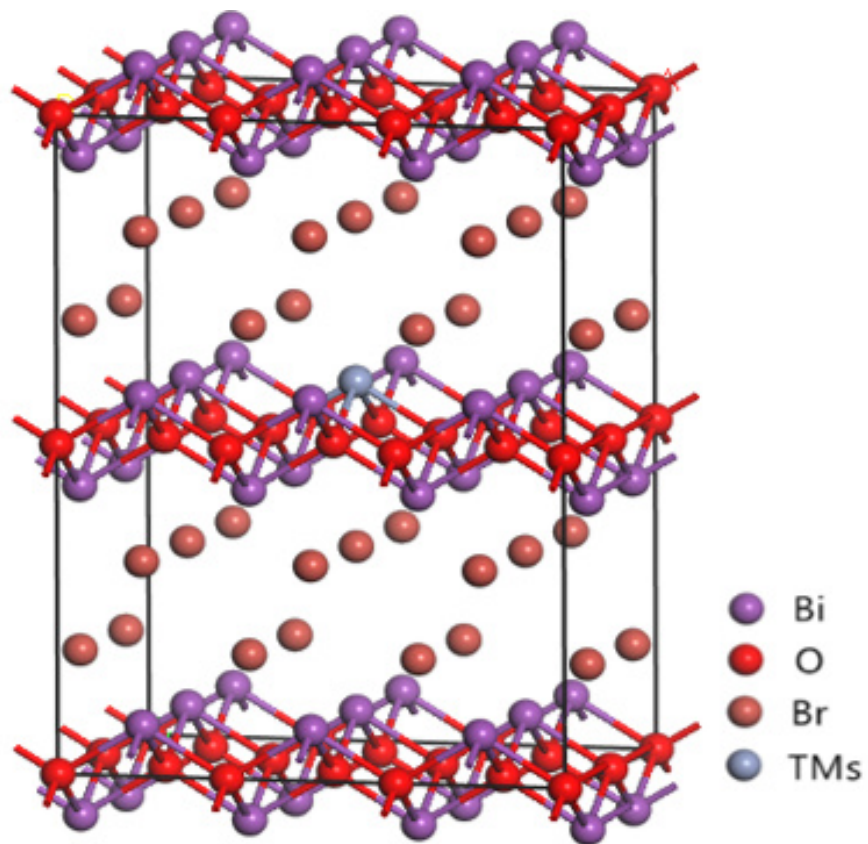
In general, the formation energies, electronic structures, optical properties and redox potentials of 3d TMs (TMs=Sc, Ti, V, Cr, Mn, Fe, Co, Ni, Cu, Zn)-doped BiOBr have been calculated based on DFT+U calculations. Firstly, the doped atoms in the BiOBr models contribute to the changes of electronic distribution and features to the varying degrees, especially, for the Ti-, V-, Cr-, Fe-, Co-, Ni-, Cu-doped BiOBr, the emergence of IELs should improve electron transition and transport efficiency, thus enhancing the visible light response ability of BiOBr. However, there is no IELs for the Sc-, Mn-, Zn-doped BiOBr, and only more electronic delocalization exists in the VB or CB regions of BiOBr. Secondly, the VB edges of V-, Fe-, Co-, Ni-, Cu-doped BiOBr shift to the more negative direction, endowed with higher oxidation ability, implying these systems possess superior redox potentials in the photocatalytic reaction. Thirdly, based on our calculated results, the priority order of photo response, structural stability and recombination probability of photoinduced carriers for 3d TMs-doped BiOBr is summarized. our theoretical findings not only can explain some experimental phenomena, but also provide significant prediction for designing and preparing high-efficient visible-light-driven BiOBr-based photocatalysts.

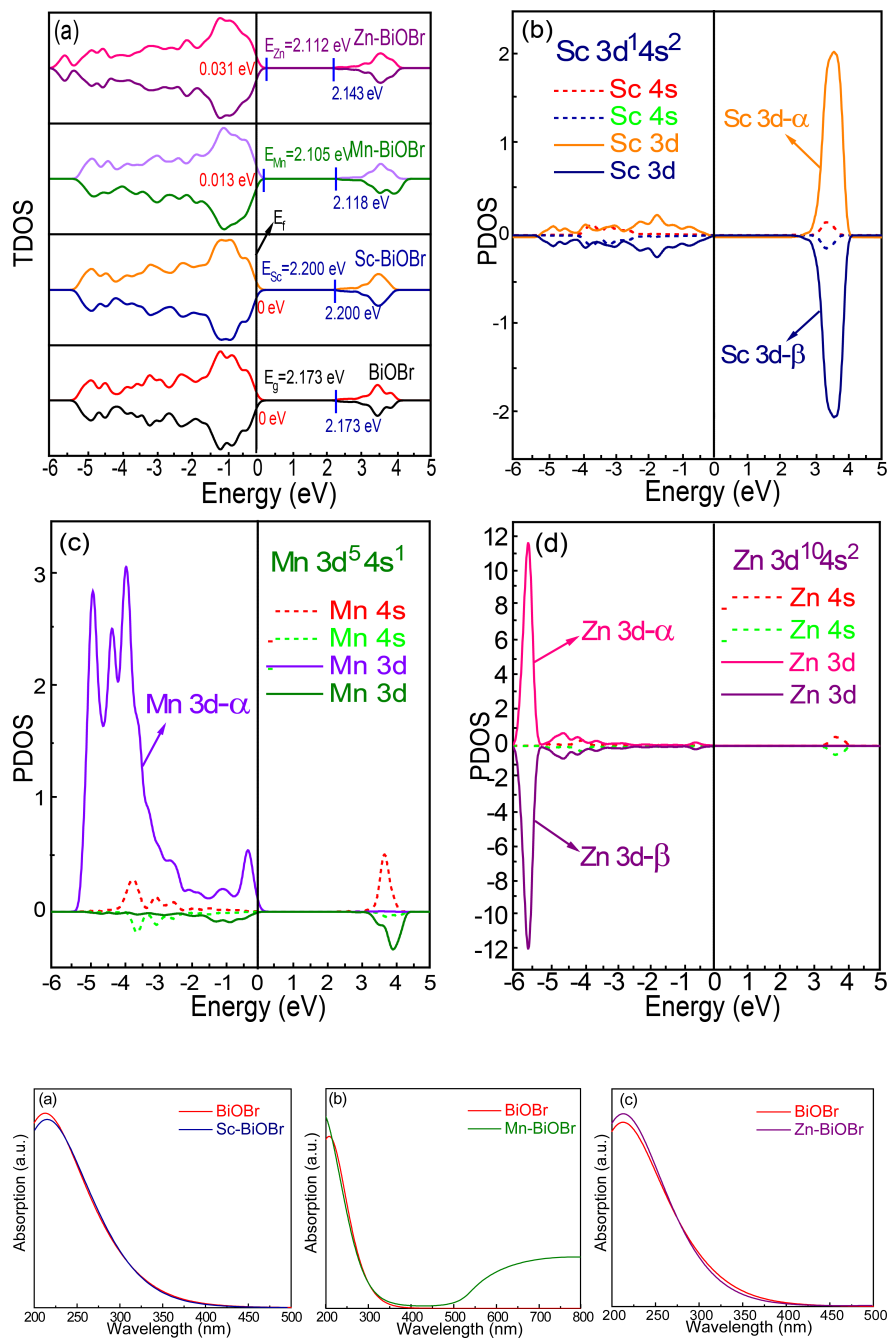
#### REFERENCES

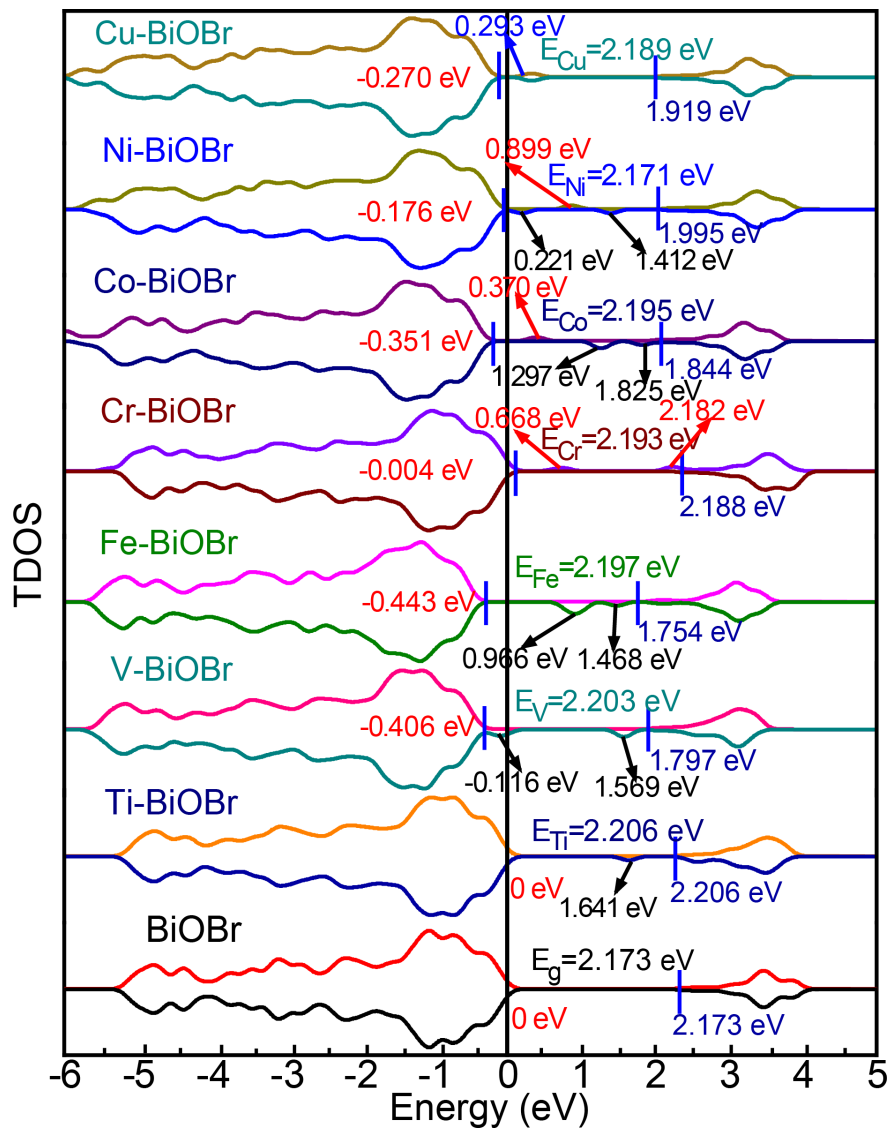
1. Q. Wang, K. Domen, Chem. Rev. **2020** , 120, 919.
2. Y.C. Bao, K.Z. Chen, Appl. Surf. Sci. **2018** , 437, 51.
3. Y. Guo, W.X. Shi, Y.F. Zhu, Y.P. Xu, F.Y. Cui, Appl. Catal. B: Environ. **2020** , 262, 118262.
4. L. Zhang, Z.K. Tang, W.M. Lau, W.J. Yin, S.X. Hu, L.M. Liu, Phys. Chem. Chem. Phys. **2017** , 19, 20968.
5. Y. Yang, C. Zhang, C. Lai, G.M. Zeng, D.L. Huang, M.Chen, J.J. Wang, F. Chen, C.Y. Zhou, W.P. Xiong, Adv. Colloid Interface Sci. **2018** , 254, 76.
6. L. Ye, Y. Su, X. Jin, H. Xie, C. Zhang, Environ. Sci.: Nano. **2014** , 1, 90-112.
7. M.Q. Yuan, F. Tian, G.F. Li, H.P. Zhao, Y.L. Liu, R. Chen, Ind. Eng. Chem. Res. **2017** , 56, 5935.
8. H. Wang, Y. Qu, Z.K. Xu, X.L. Zhang, X.X. Zhang, F. Yang, L.Q. Jing, Sci. China Mater. **2018** , 62, 653.
9. W. Zhou, J.K. Guo, S. Shen, J. Pan, S.F. Yin, Acta Phys.-Chim. Sin. **2020** , 36, 11.

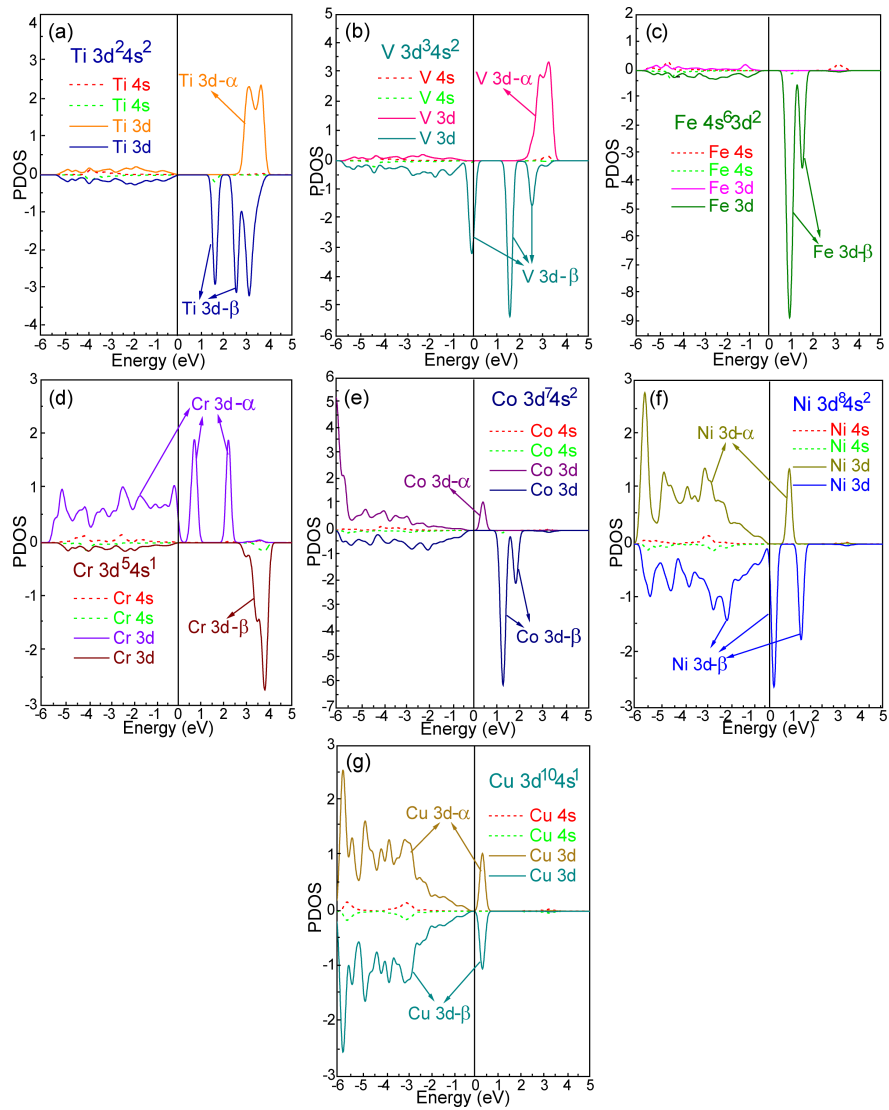
10. R.J. Wang, G.H. Jiang, X.H. Wang, R.B. Hu, X.G. Xi, S.Y. Bao, Y. Zhou, T. Tong, S. Wang, T. Wang, W.X. Chen, *Powder Technol.* **2012** , 228, 258.
11. G.H. Jiang, R.J. Wang, X.H. Wang, X.G. Xi, R.B. Hu, Y. Zhou, S. Wang, T. Wang, W.X. Chen, *ACS Appl. Mater. Inter.* **2012** , 4, 4440
12. Z. Wei, G.H. Jiang, L. Shen, X. Li, X.H. Wang, W.X. Chen, *MRS Commun.***2013** , 3, 145.
13. G.H. Jiang, X.H. Wang, Z. Wei, X. Li, X.G. Xi, R.B. Hu, B.L. Tang, R.J. Wang, S. Wang, T. Wang, W.X. Chen, *J. Mater. Chem. A.***2013** , 1, 2406.
14. W. Huang, X. Hua, Y. Zhao, K. Li, L. Tang, M. Zhou, Z. Cai, *Journal of Mater. Sci.: Mater. El.* **2019** , 30, 14967.
15. J.Q. Guo, X. Liao, M.H. Lee, G. Hyett, C.C. Huang, D.W. Hewak, S. Mailis, W. Zhou, Z. Jiang, *Appl. Catal. B: Environ.* **2019** , 243, 502.
16. W.B. Zhang, S.J. Chen, M.L. He, G.Q. Zhu, W. Yang, Y.H. Tian, Z.J. Zhang, S.L. Zhang, F.C. Zhang, Q.F. Wu, *Mater. Res. Express.***2018** , 5, 075512.
17. L.H. Shao, Y.T. Liu, L.L. Wang, X.N. Xia, X.Y. Shen, *Appl. Surf. Sci.***2020** , 502, 143895.
18. X.C. Zhang, J.B. Wei, R. Li, C.M. Zhang, H. Zhang, P.D. Han, C.M. Fan, *J. Mater. Sci.* **2017** , 53, 4494.
19. J. Ketterer, V. Kramer, *Acta. Cryst.* **1986** , 42, 1098.
20. C.H. Ding, Z.Y. Ma, C.Q. Han, X.X. Liu, Z.Y. Jia, H.Q. Xie, K.Y. Bao, L.Q. Ye, *J. Taiwan Inst. Chem. Eng.* **2017** , 78, 395.
21. S.J. Clark, M.D. Segallii, C.J. Pickardii, P.J. Hasnipiii, M.I.J.J.Z.F.K. Probertiv, *Z. Kristallogr.* **2005** , 220, 567.
22. J. Pack, H. Monkhorst, D. Freeman, *Solid State Commun.* **1979** , 29, 723.
23. H. Lee, M.Y. Jeong, J.-H. Sim, H. Yoon, S. Ryee, M.J. Han, *EPL.***2019** , 125, 47005.
24. Z.Y. Zhao, W.W. Dai, *Inorg. Chem.* **2014** , 53, 13001.
25. Q.L. Liu, Z.Y. Zhao, Q.J. Liu, *Mat. Sci. Semicon. Proc.* **2015** , 33, 94.
26. T.P. Kaloni, *J. Phys. Chem. C.* **2014** , 118, 25200.
27. Z.H. Levine, D.C. Allan, *Phys. Rev. Lett.* **1989** , 63, 1719.
28. W.L. Huang, Q.S. Zhu, *J. comput. Chem.* **2009** , 30, 183.
29. X. Zhang, Z.H. Ai, F.L. Jia, L.Z. Zhang, *J. Phys. Chem. C.***2008** , 112, 747.
30. Q. Fan, X. Chen, F. Chen, J. Tian, C. Yu, C. Liao, *Appl. Surf. Sci.***2019** , 481, 564.
31. C. Stampfl, C.G. Van de Walle, *Phys. Rev. B.* **1999** , 59, 5521.
32. T. Li, X.C. Zhang, C.M. Zhang, R. Li, J.X. Liu, R. Lv, H. Zhang, P.D. Han, C.M. Fan, Z.F. Zheng, *Phys. Chem. Chem. Phys.* **2019** , 21, 868.
33. N.A. Putri, V. Fauzia, S. Iwan, L. Roza, A.A. Umar, S. Budi, *Appl. Surf. Sci.* **2018** , 439, 285.
34. L. Yosefi, M. Haghghi, *Mater. Res. Bull.* **2019** , 113, 51.
35. Y.L. Geng, N. Li, J.Y. Ma, Z.H. Sun, *J. Energy Chem.* **2017** , 26, 416.
36. S.X. Zhou, T.T. Shi, Z.H. Chen, D.S. Kilin, L.L. Shui, M.L. Jin, Z.C. Yi, M.Z. Yuan, N. Li, X.B. Yang, Q.G. Meng, X. Wang, G.F. Zhou, *Catalysts.* **2019** , 9, 198.
37. B. Ge, L. Han, X. Liang, F. Li, X. Pu, X. Zhu, Z. Zhang, X. Shao, C. Jin, W. Li, *Appl. Surf. Sci.* **2018** , 462, 583.
38. W.T. Li, Y.B. Zou, X. Geng, F. Xiao, G.Y. An, D.S. Wang, *Mol. Catal.***2017** , 438, 19.
39. Y. Liu, J. Li, J.Y. Li, X.H. Yan, F.D. Wang, W.N. Yang, D.H.L. Ng, J. Yang, *J. Clean. Prod.* **2020** , 252, 119573.
40. C.S. Guo, S.W. Gao, J.P. Lv, S. Hou, Y. Zhang, J. Xu, *Appl. Catal. B: Environ.* **2017** , 205, 68.
41. J. Jiang, F.F. Sun, S. Zhou, W. Hu, H. Zhang, J.C. Dong, Z. Jiang, J.J. Zhao, J.F. Li, W.S. Yan, M. Wang, *Nat. Commun.* **2018** , 9, 2885.
42. Z.Y. Zhao, Z.S. Li, Z.G. Zou, *Phys. Chem. Chem. Phys.* **2011** , 13, 4746.
43. B.X. Li, L.Z. Shao, R.S. Wang, X.P. Dong, F.G. Zhao, P. Gao, Z.Q. Li, *J. Mater. Chem. A.* **2018** , 6, 6344.
44. S.M. Chang, W.S. Liu, *Appl. Catal. B: Environ.* **2011** , 101, 333-342.
45. F. Opoku, K.K. Govender, C.G.C.E. van Sittert, P.P. Govender, *ChemistrySelect.* **2017** , 2, 6304.

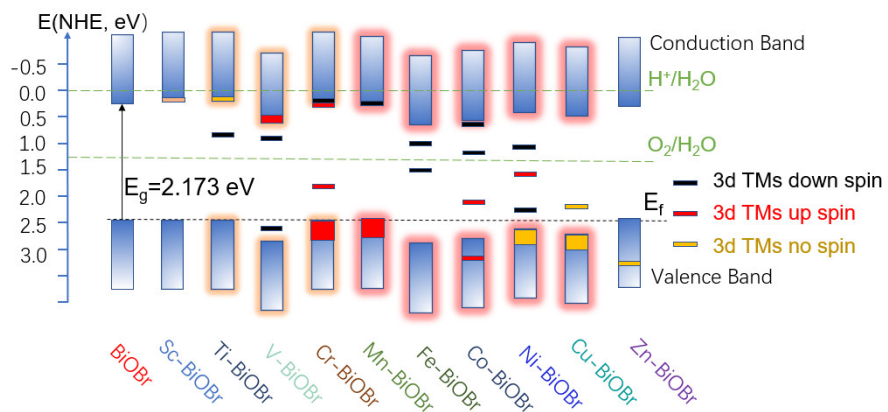
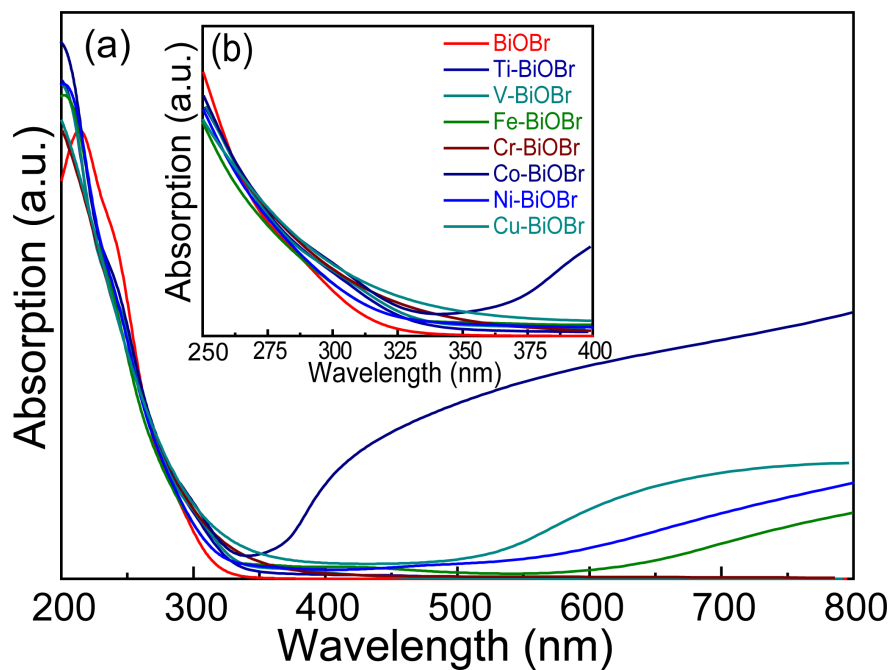
46. Y. Porte, R. Maller, H. Faber, H.N. AlShareef, T.D. Anthopoulos, M.A. McLachlan, J. Mater. Chem. C. **2016** , 4, 758.

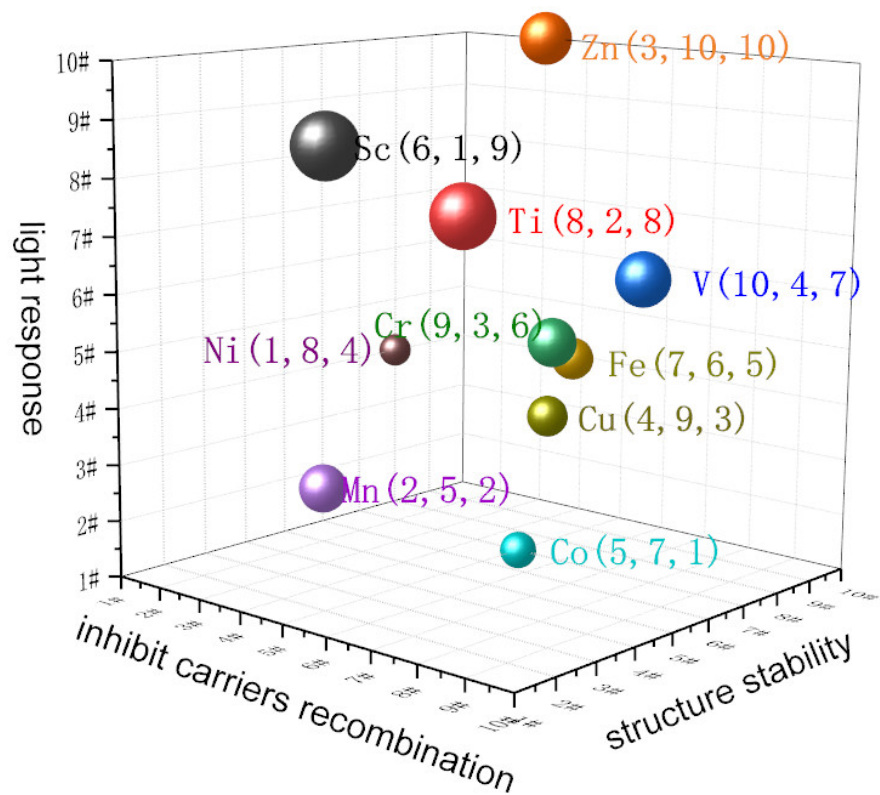
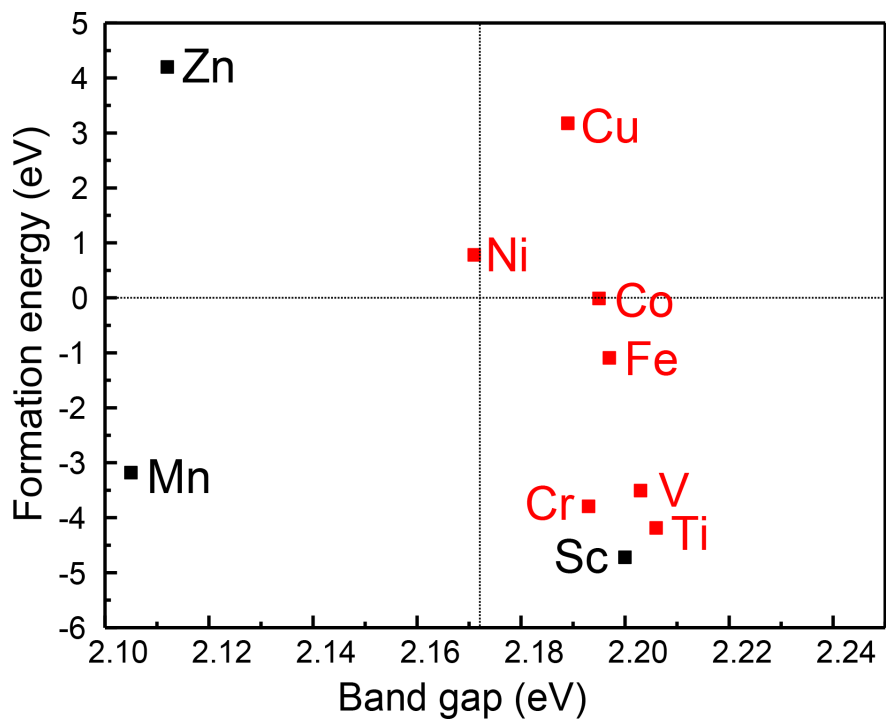












Hosted file

TABLE 1 docx.docx available at <https://authorea.com/users/349781/articles/474760-regulating-electronic-properties-of-biobr-to-enhance-visible-light-response-via-3d-transition-metals-doping-dft-u-calculations>

### Hosted file

TABLE 2 .docx available at <https://authorea.com/users/349781/articles/474760-regulating-electronic-properties-of-biobr-to-enhance-visible-light-response-via-3d-transition-metals-doping-dft-u-calculations>